Extended reduced-order surrogate models for scalar-tensor gravity in the strong field and applications to binary pulsars and gravitational waves

Minghao Guo,[1,*] Junjie Zhao,[2] and Lijing Shao[3,4,†]

[1]*Peking University, Beijing 100871, China*
[2]*School of Physics and State Key Laboratory of Nuclear Physics and Technology, Peking University, Beijing 100871, China*
[3]*Kavli Institute for Astronomy and Astrophysics, Peking University, Beijing 100871, China*
[4]*National Astronomical Observatories, Chinese Academy of Sciences, Beijing 100012, China*

(Dated: June 4, 2021)

We investigate the scalar-tensor gravity of Damour and Esposito-Farèse (DEF) with spontaneous scalarization phenomena developed for neutron stars (NSs). Instead of solving the modified Tolman-Oppenheimer-Volkoff equations for slowly rotating NSs via the shooting method, we construct a reduced-order surrogate model to predict the relations of mass, radius, moment of inertia, effective scalar coupling, and two extra coupling parameters of a NS to its central matter density. We code the model in the `pySTGROMX` package that speeds up the calculations at two and even three orders of magnitude and yet still keeps accuracy at $\sim 1\%$ level. Using the package, we can predict *all* the post-Keplerian parameters in the timing of binary pulsars conveniently, which allows us to place comprehensive constraints on the DEF theory in a quick and sound way. As an application, we perform Markov-chain Monte Carlo simulations to constrain the parameters of the DEF theory with well-timed binary pulsars. Utilizing five NS-white dwarf and three NS-NS binaries, we obtain the most stringent constraints on the DEF theory up to now. Our work provides a public tool for quick evaluation of NSs' derived parameters to test gravity in the strong-field regime.

I. INTRODUCTION

Albert Einstein's theory of general relativity (GR) [1] remains the most accurate theory of gravity for more than a century. This elegant theory has passed all tests with flying colors from, e.g., the Solar System experiments [2], cosmological observation [3], the timing of binary pulsars [4–6], and gravitational waves (GWs) from coalescing binary black holes (BBHs) [7–10] and binary neutron stars (BNSs) [11–13]. From the Earth up to the Universe, from weak to strong gravitational field, GR remains the gold standard.

There are good theoretical reasons to go beyond GR, however [14]. Therefore, even with the success of GR, considerable efforts are still being made for alternative theories of gravity (see Refs. [2, 15] for a review). In GR, gravity is mediated solely by a massless, spin-2 tensor field, namely the metric of spacetime $g_{\mu\nu}$. Differently from GR, scalar-tensor theories of gravity, as natural alternatives, add one or more extra scalar degrees of freedom in the gravitational sector. They not only arise naturally as a possible low-energy limit of higher dimensional theories, such as Kaluza-Klein theory [16, 17] and string theories [18], but also have a potential connection to the inflation, the dark energy, and a yet unknown unified theory of quantum gravity [3]. Originally suggested by Scherrer in 1941 [19], the most popular scalar-tensor gravity theories are developed in a modern framework by Jordan [20, 21], Fierz [22], Brans and Dicke [23] (JFBD; see a review in Ref. [18]). JFBD-like theories, as metric theories of gravity, do not violate the weak equivalence principle but the strong equivalence principle (SEP) due to the nonminimally coupled scalar field in the Einstein-Hilbert action [6, 15]. Tests of SEP, which is the heart of GR, provide a powerful tool to experimentally constrain these theories.

In this paper, we restrict our attention to a class of special JFBD-like gravity formulated by Damour and Esposito-Farèse (DEF) [24–26], where prominent violations of the SEP due to *nonperturbative strong-field effects* are known to arise. The DEF theory can pass present weak-field gravitational tests, such as the Cassini experiment [27], but exhibits very significant strong-field deviations away from GR in the systems involving strongly self-gravitating neutron stars (NSs) [25, 28].

In the weak-field regime, scalar-tensor theories have been extensively investigated, mostly from experiments in the Solar System, like the Cassini probe and other space missions [27]. In the parametrized post-Newtonian (PPN) framework, it is confirmed to a high precision $\sim 10^{-5}$ for the Eddington-Robertson-Schiff parameters [15], indicating that the DEF theory is compatible with the weak-field tests when its weak-field coupling parameter, α_0, is small.

However, in the strong-field regime for the DEF theory, one kind of nonperturbative strong-field effects, the so-called *spontaneous scalarization*, occurs as a scalar analogue of the phase transition in ferromagnetism [25, 26, 29]. It naturally arises in an isolated compact star such as a NS under a certain condition with the scalar field excited far above its background value. Such deviation from GR introduces considerable modifications into the properties of scalarized compact stars. It also affects the relativistic orbital motion if a scalarized NS is in a binary, via, e.g., a body-dependent effective gravitational constant, extra gravitational binding energy related to the scalar field, and dipolar radiation in addition to the canonical quadrupolar radiation in GR [24, 30]. Long-term monitoring of binary pulsars and transient observations of GWs from BNS coalescences are therefore powerful tools to probe the contribution from spontaneous scalarization in extreme environments of strong gravitational fields [5, 26, 31].

The high-precision timing of binary pulsars provides some

* Corresponding author: gmh@pku.edu.cn
† Corresponding author: lshao@pku.edu.cn

of the tightest gravity tests with strongly self-gravitating bodies in the quasi-stationary strong-field gravity regime [4–6, 32]. In this regime, gravitational fields are strong with large spacetime curvature in the vicinity of the NSs while the typical velocity v is much smaller than the speed of light c with a ratio of $v/c \sim 10^{-3}$. To extract the information from pulsar timing for testing gravity theories, the parametrized post-Keplerian (PPK) formalism was developed as a generic pulsar timing model [33]. The dynamical information can be obtained from the pulsar timing and pulse-structure data by fitting the data to a model consisting of a set of theory-independent Keplerian and post-Keplerian timing parameters. The PPK formalism is a powerful tool and makes it possible to provide constraints on a variety of alternative gravity theories.

In the DEF theory, one of the PPK parameters, $\dot{P}_b$, which is related to binary orbital decay, is modified due to the extra dipolar radiation [24]. The dipolar contribution, corresponding to a -1 post-Newtonian (PN) correction,[1] may dominate the radiation when v/c is small. Thus, at the early time of the binary system, due to a small $v/c \sim 10^{-3}$, this mechanism enhances the energy flux of GWs emitted from the system and thus changes $\dot{P}_b$ in a noticeable way. In addition, the DEF theory predicts that, due to the spontaneous scalarization, *all* the PPK parameters are modified from the GR prediction [33], thus these parameters can be combined to constrain the DEF theory [26].

With the detection of GW events, especially coalescing BNSs, GW170817 [11] and a possible candidate GW190425 [34] up to date, we have a new testbed in probing the strong-field gravity. In the late inspiral stage, the spacetime of BNSs is strongly curved and highly dynamical in the vicinity of NSs, providing a powerful laboratory in the highly dynamical strong-field regime. Matched-filter analyses, used in parameter estimation of GWs [35], are sensitive to GW phase evolution, which is modified in the DEF theory and can be distinguished from GR. Thus, GW signals can also be utilized to bound the DEF theory.

So far, however, limited by the sensitivity of the LIGO/Virgo detectors below tens of hertz, the bound on dipolar radiation from GW170817 is still looser than that from the timing of binary pulsars [28, 36], since dipolar radiation corresponds to a -1 PN correction and plays a relatively important role when $v/c \ll 1$. Future ground-based and space-based GW detectors with a better low-frequency sensitivity, such as Cosmic Explorer (CE) [37], Einstein Telescope (ET) [38], DECi-hertz Interferometer Gravitational wave Observatory (DECIGO) [39] and Decihertz Observatory (DO) [40, 41] will place tighter constraints on gravity theories by either extending the sensitivity bands to be below 10 Hz or increasing the sensitivity further (see e.g. Ref. [42]).

To perform tests on the scalar-tensor gravity, first, one must derive the relevant predictions on observations precisely. The predictions on some properties of a NS, such as its radius R, mass m_A, moment of inertia I_A, and the scalar coupling parameter α_A, are derived by numerically integrating the modified Tolman-Oppenheimer-Volkoff (mTOV) equations of a slowly rotating NS with the shooting method [25, 26]. This integration depends on the equation of state (EOS) of NS matters, which is still full of large uncertainties (see e.g. Refs. [43, 44]).

Apart from the NSs' properties above, many PPK parameters in binary pulsars, such as the periastron advance rate and Einstein delay parameter, require other derived properties of NSs in the DEF theory. They consist of the coupling parameters β_A and k_A, which are predicted by calculating the derivatives of scalar coupling α_A and moment of inertia I_A, with respect to the scalar field at infinity [26]. Note that the calculations of β_A and k_A should be performed for a fixed value of baryonic mass $\bar{m}_A$. This procedure requires the shooting method for both $\bar{m}_A$ and the scalar field simultaneously [26]. The calculations for such parameters are very time-consuming and thus expensive for large-scale computation.

In practice, to constrain the free parameters in the DEF theory with the well-timed pulsars in a statistically sound way, we use Bayesian inference through Markov-chain Monte Carlo (MCMC) simulations. This approach requires the evaluation of the likelihood function hundreds of thousands to millions of times. Each step of MCMC simulation requires the corresponding NS properties derived from the integration of the mTOV equations with the shooting method. The whole simulation is thus time-consuming and expensive. Such computationally intensive studies have been conducted in Ref. [28] for the first time.

In this study, instead of solving the mTOV equation iteratively and repeatedly by trial and error, we build a reduced-order surrogate model (ROM) to predict NS properties. The surrogate model is very quick by a linear algebraic operation rather than the iterative integration. Following the earlier work of Zhao *et al.* [36], we extend our model to predict all the PPK parameters, not just the orbital period decay parameter $\dot{P}_b$. To explore EOS-dependent aspects, in this work, we choose 15 EOSs that are all consistent with the maximum mass of NSs being larger than $2\,\mathrm{M}_\odot$. This extends the number of EOSs in Ref. [36]. We use the central matter density ρ_c of a NS to predict its radius R, mass m_A, moment of inertia I_A and its derivative k_A, as well as the effective scalar coupling α_A and its derivative β_A. Our models are at $\sim 1\%$ level of accuracy. According to our performance tests, one can speed up the calculations by at least two and even three orders of magnitude for the coupling parameters β_A and k_A, and yet still keep the due accuracy. We demonstrate various applications with binary pulsars to illustrate the practical value of our ROMs.

The improvements of this work include the followings.

(I) We use a larger set of EOSs.

(II) We calculate the mTOV equation to build ROMs in the DEF theory for slowly rotating NSs, instead of the non-rotating ones, to predict the moment of inertia and its derivative.

(III) We extend our ROMs to the coupling parameters by calculating the derivatives of α_A and I_A, and thus we can

[1] We refer a correction at n PN order to $O(v^{2n}/c^{2n})$ modification relative to the Newtonian order. For GWs, the quadrupolar radiation is denoted as 0 PN, and the dipolar radiation is at -1 PN.

predict all the PPK parameters with new ROMs.

(IV) Our ROMs speed up the calculation by two to even three orders of magnitude.

(V) We utilize the binary pulsars including double NSs to derive tight constraints on the DEF theory.

The rest of this paper is organized as follows. Section II briefly reviews the nonperturbative spontaneous-scalarization phenomena for slowly rotating NSs. The modifications of orbital period decay, periastron advance rate, and Einstein delay parameter in the DEF gravity are discussed. In Sec. III, we analyze the difficulties in solving the mTOV equations and calculating the derived parameters for large-scale calculations. We develop a better numerical method and code it in the `pySTGROMX` (a.k.a. `pySTGROM eXtension`) package which is public for easy use for the community.[2] In Sec. IV, with the speedup from `pySTGROMX`, we constrain the DEF theory tightly by combining the relevant PPK parameters available from observations of five NS-white dwarf (WD) systems and three NS-NS systems. Discussions and conclusions are given in Sec. V.

II. SPONTANEOUS SCALARIZATION IN THE DEF THEORY

The DEF theory is defined by the following general action in the *Einstein frame* [25, 26],

$$S = \frac{c^4}{16\pi G_\star}\int \frac{\mathrm{d}^4x}{c}\sqrt{-g_\star}\left[R_\star - 2g_\star^{\mu\nu}\partial_\mu\varphi\partial_\nu\varphi - V(\varphi)\right] + S_m\left[\psi_m; A^2(\varphi)g^\star_{\mu\nu}\right]. \tag{1}$$

Here, $G_\star$ denotes the bare gravitational constant, $g_\star \equiv \det g^\star_{\mu\nu}$ is the determinant of "Einstein metric" $g^\star_{\mu\nu}$, $R_\star$ is the Ricci curvature scalar of $g^\star_{\mu\nu}$, and φ is a dynamical scalar field. In the last term of Eq. (1), ψ_m denotes matter fields collectively, and the conformal coupling factor $A(\varphi)$ describes how φ couples to ψ_m in the Einstein frame. We assume that the potential, $V(\varphi)$, is a slowly varying function at the typical scale of the system we consider and set $V(\varphi) = 0$ in our calculation for simplicity (see Refs. [45, 46] for a massive scalar field).

Varying the action (1) yields the field equations,

$$R^\star_{\mu\nu} = \partial_\mu\varphi\partial_\nu\varphi + \frac{8\pi G_\star}{c^4}\left(T^\star_{\mu\nu} - \frac{1}{2}T^\star g^\star_{\mu\nu}\right), \tag{2}$$

$$\Box_{g^\star}\varphi = -\frac{4\pi G_\star}{c^4}\alpha(\varphi)T_\star, \tag{3}$$

where $T^{\mu\nu}_\star \equiv 2c(-g_\star)^{-1/2}\delta S_m/\delta g^\star_{\mu\nu}$ denotes the matter stress-energy tensor, and $T^\star \equiv g^\star_{\mu\nu}T^{\mu\nu}_\star$ is the trace. In Eq. (3), the parameter $\alpha(\varphi)$ is defined as the derivative of logarithmic $A(\varphi)$,

$$\alpha(\varphi) \equiv \frac{\partial \ln A(\varphi)}{\partial\varphi}, \tag{4}$$

which indicates the coupling strength between the scalar field and matters [see Eq. (3)].

In the DEF theory [26], $\ln A(\varphi)$ is designated as

$$\ln A(\varphi) = \frac{1}{2}\beta_0\varphi^2. \tag{5}$$

Then $\alpha(\varphi) = \partial \ln A(\varphi)/\partial\varphi = \beta_0\varphi$. We denote $\alpha_0 \equiv \beta_0\varphi_0$, where φ_0 is the asymptotic scalar field value of φ at spatial infinity. Note that we have $\alpha_0 = \beta_0 = 0$ in GR.

For NSs, nonperturbative scalarization phenomena develop when [25, 47]

$$\beta_0 \equiv \left.\frac{\partial^2 \ln A(\varphi)}{\partial\varphi^2}\right|_{\varphi=\varphi_0} \lesssim -4. \tag{6}$$

Generally, a more negative β_0 means more manifest spontaneous scalarization in the strong-field regime. In such case, the *effective scalar coupling* for a NS "A" with a total mass-energy of m_A is

$$\alpha_A \equiv \left.\frac{\partial \ln m_A(\varphi)}{\partial\varphi}\right|_{\varphi=\varphi_0}, \tag{7}$$

which measures the effective coupling strength between the scalar field and the NS.

Now we consider a scalarized NS in a binary system in the DEF theory. For a binary pulsar system with the pulsar labeled "A" and its companion labeled "B", the parameters α_A and α_B contribute to the secular change of the orbital period [26]. In this work, we investigate two contributions to $\dot{P}_b$, the dipolar contribution, $\dot{P}_b^{\rm dipole}$, and the quadrupolar contribution, $\dot{P}_b^{\rm quad}$. They are defined by [26]

$$\dot{P}_b^{\rm dipole} = -\frac{2\pi G_\star n_b}{c^3}g(e)\frac{m_A m_B}{m_A+m_B}(\alpha_A-\alpha_B)^2, \tag{8}$$

$$\dot{P}_b^{\rm quad} = -\frac{192\pi G_{AB}^{5/3}n_b^{5/3}}{5c^5(1+\alpha_A\alpha_B)}f(e)\frac{m_A m_B}{(m_A+m_B)^{1/3}}, \tag{9}$$

where $n_b \equiv 2\pi/P_b$, and

$$g(e) \equiv \left(1-e^2\right)^{-5/2}\left(1+\frac{e^2}{2}\right), \tag{10}$$

$$f(e) \equiv \left(1-e^2\right)^{-7/2}\left(1+\frac{73}{24}e^2+\frac{37}{94}e^4\right). \tag{11}$$

Here the bare gravitational constant in Eq. (8), $G_\star$, is obtained with the Newtonian constant G_N by $G_\star = G_N/(1+\alpha_0^2)$ [24], owing to the weak field coupling. The body-dependent effective gravitational constant in Eq. (9), G_{AB}, is given by $G_{AB} \equiv G_\star(1+\alpha_A\alpha_B)$. The quadrupolar contribution $\dot{P}_b^{\rm quad}$ is close to the prediction of GR with a negligible correction, while the dipolar contribution $\dot{P}_b^{\rm dipole}$ is the dominant additional contribution in the DEF theory. Other subleading contributions induced by the scalar field can be neglected in this study [see Eq. (6.52) of Ref. [24]]. Note that the effective scalar coupling is zero for BHs in the DEF theory due to the no-hair theorem [8, 14] and approaches to α_0 for WDs in the weak field. Thus, considering Eq. (8), the contribution

[2] https://github.com/mh-guo/pySTGROMX

of dipolar radiation to $\dot{P}_b$ plays an important role in NS-WD, NS-BH, and asymmetric NS-NS binaries. In those binaries, there could be a large difference between α_A and α_B.

Similarly to α_A, we define

$$\beta_A \equiv \left.\frac{\partial \alpha_A}{\partial \varphi}\right|_{\varphi=\varphi_0}, \tag{12}$$

which is the strong-field analogue of the parameter β_0. Then the theoretical prediction for the periastron advance rate in the DEF theory is [26]

$$\dot{\omega}^{\rm th}(m_A, m_B) \equiv \frac{3n_b}{1-e^2}\left(\frac{G_{AB}(m_A+m_B)n_b}{c^3}\right)^{2/3} \times\left[\frac{1-\frac{1}{3}\alpha_A\alpha_B}{1+\alpha_A\alpha_B} - \frac{X_A\beta_B\alpha_A^2 + X_B\beta_A\alpha_B^2}{6(1+\alpha_A\alpha_B)^2}\right], \tag{13}$$

where $X_A \equiv m_A/(m_A+m_B) \equiv 1 - X_B$. Finally, we consider a slowly-rotating NS with moment of inertia (in Einstein units) I_A. We denote

$$k_A \equiv -\left.\frac{\partial \ln I_A}{\partial \varphi}\right|_{\varphi=\varphi_0}, \tag{14}$$

as the "coupling factor" for moment of inertia [26]. The theoretical prediction of the Einstein delay parameter in the DEF theory is [26],

$$\gamma^{\rm th}(m_A, m_B) \equiv \frac{e}{n_b}\frac{X_B}{1+\alpha_A\alpha_B}\left(\frac{G_{AB}(m_A+m_B)n_b}{c^3}\right)^{2/3} \times\left[X_B(1+\alpha_A\alpha_B) + 1 + K_A^B\right], \tag{15}$$

where $K_A^B \equiv \alpha_B(m_B)k_A(m_A)$ describes the contribution from the variation of I_A under the influence of the companion B.

For the (almost) symmetric double NS systems, such as the double pulsar PSR J0737−3039 [48], because of the similar binary masses, α_A is very close to α_B, leading to a tiny effect from the dipolar radiation. Thus, it could be difficult to constrain the DEF theory solely by the PPK parameter $\dot{P}_b$, unless $\dot{P}_b$ is extremely well measured. For these systems, instead of $\dot{P}_b$, the PPK parameters $\dot{\omega}$ and γ can be used of to provide better constraints, especially when both of the NSs develop spontaneous scalarization.

III. EXTENDED ROM MODELS

A. Solving the mTOV equations

We here turn our attention to deriving the quantities of NSs in the strong field. For a specific EOS, given the initial conditions, namely the central matter density ρ_c and the central scalar field φ_c, one can integrate the mTOV equations to obtain the solution of a slowly rotating NS. To derive the prediction of a DEF theory (namely, with fixed α_0, β_0), one varies the initial condition φ_c iteratively with the "shooting method" until the boundary solution matches the desired value of $\varphi_0 = \alpha_0/\beta_0$. Thus, given parameter set (α_0, β_0, ρ_c), one can solve the mTOV equation by the shooting method to obtain the macroscopic quantities of a NS (see Ref. [26] for details). The quantities contain the NS radius R, the gravitational mass m_A, the baryonic mass $\bar{m}_A$, the effective scalar coupling α_A, and the moment of inertia I_A. In this way, we have a comprehensive description of the spontaneous scalarization. In Fig. 1, we show mass-radius relation of NSs in a DEF theory with $\log_{10}|\alpha_0| = -5.0$ and $\beta_0 = -4.5$ for 15 EOSs we adopt in this study. It indicates clearly that the spontaneous scalarization phenomena develop for NSs with certain masses, and larger radii are predicted in this range.

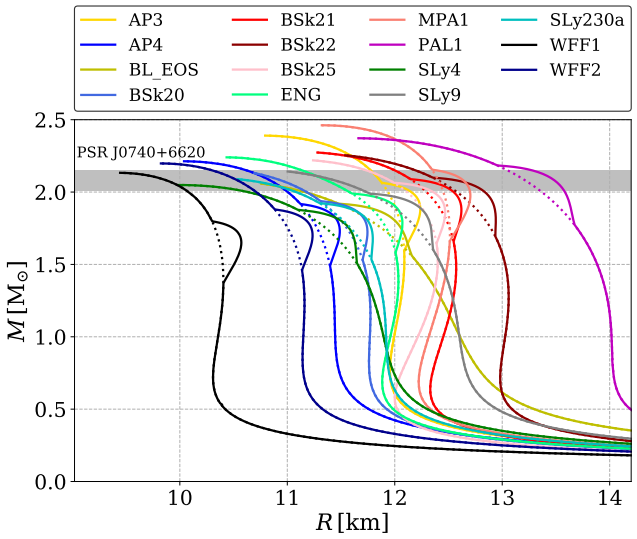

FIG. 1. Mass-radius relations of NSs for the 15 EOSs that we adopt in this study. The mass-radius relations are derived from GR (dashed lines) and from a DEF theory with $\log_{10}|\alpha_0| = -5.0$ and $\beta_0 = -4.5$ (solid lines). The massive pulsar mass from PSR J0740+6620 [49] is overlaid in gray.

However, to determine the coupling parameters β_A and k_A, we have to calculate the derivatives with respect to the scalar field φ_0 from Eqs. (12) and (14) for a fixed form of the conformal coupling factor $A(\varphi)$ (i.e., with a fixed β_0) and a fixed baryonic mass $\bar{m}_A$. Calculations with different φ_0's (or equivalently, different α_0's) but the same β_0 and $\bar{m}_A$ are required. For a single run, the calculation is generally performed by applying the shooting method for both φ_0 and $\bar{m}_A$ with trial and error [26]. Therefore, obtaining β_A and k_A is usually very time-consuming, especially for a large-scale calculation. In this study, since we investigate the phenomena in the whole parameter space of interest, we calculate the relevant derivatives on a grid covering the region to avoid wasteful repetition.

In practice, for each EOS, we choose the range of ρ_c so that $m_A \in (1\,{\rm M}_\odot, m_A^{\rm max})$ with the EOS-dependent maximum NS mass $m_A^{\rm max}$. We set an uneven spacing of ρ_c in this range. The spacing of ρ_c samples is smaller in the range where the coupling parameters α_A, β_A and k_A are rapidly changing. The number of samples in ρ_c, namely N_{ρ_c}, varies from $\sim$ 300 to $\sim$ 500, depending on the specific EOS. Then we generate an

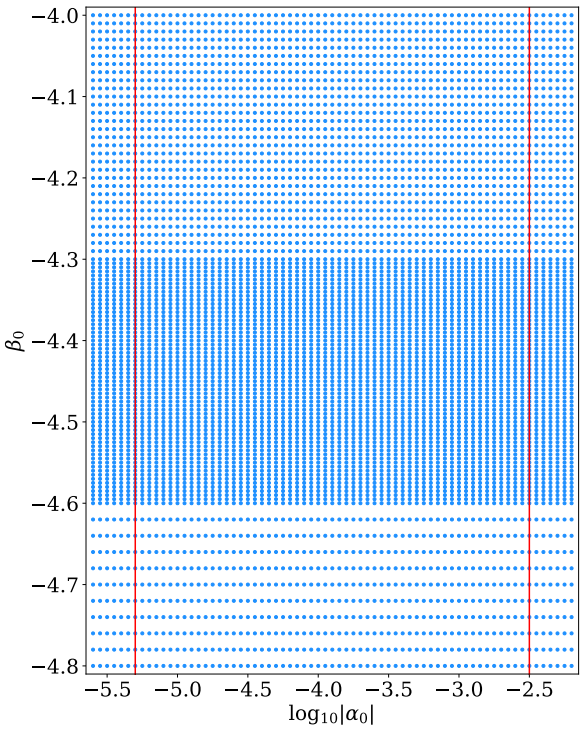

FIG. 2. An uneven grid in the parameter space $(\log_{10}|\alpha_0|, -\beta_0)$ for calculating β_A and k_A. We generate a set of $69 \times 101 = 6969$ parameter pairs as the training data in total. The region between red lines corresponds to the data we use for building ROMs.

uneven gird of $(\log_{10}|\alpha_0|, \beta_0) \in [-5.6, -2.2] \times [-4.8, -4.0]$, as shown in Fig. 2. The number of nodes in grid is set to $N_{\alpha_0} \times N_{\beta_0} = 69 \times 101 = 6969$. We calculate the coupling parameters β_A and k_A on each point with a reasonable differential step. Specifically, for each point $(\alpha_0, \beta_0, \rho_c)$, we carefully select backward step $\Delta\varphi_0^{(1)}$ and forward step $\Delta\varphi_0^{(2)}$. Thus, we have $\varphi_0^{(1)} = \varphi_0 - \Delta\varphi_0^{(1)}$ and $\varphi_0^{(2)} = \varphi_0 + \Delta\varphi_0^{(2)}$, or equivalently, $\alpha_0^{(1)}$ and $\alpha_0^{(2)}$. Then we select points $\left(\alpha_0^{(1)}, \beta_0, \rho_c^{(1)}\right)$ and $\left(\alpha_0^{(2)}, \beta_0, \rho_c^{(2)}\right)$, where $\rho_c^{(1)}$ and $\rho_c^{(2)}$ are chosen so that $\bar{m}_A$ can be fixed to the value of $\bar{m}_A$ at the point $(\alpha_0, \beta_0, \rho_c)$. By interpolating the samples, we obtain the values $\alpha_A^{(1)}$, $\alpha_A^{(2)}$, $I_A^{(1)}$, and $I_A^{(2)}$ at these two points. Then we calculate β_A and k_A numerically following

$$\beta_A = \frac{\alpha_A^{(2)} - \alpha_A^{(1)}}{\varphi_0^{(2)} - \varphi_0^{(1)}}, \tag{16}$$

and

$$k_A = -\frac{\ln I_A^{(2)} - \ln I_A^{(1)}}{\varphi_0^{(2)} - \varphi_0^{(1)}}. \tag{17}$$

Finally, we make use of the data of $\log_{10}|\alpha_0| \in [-5.3, -2.5]$, instead of $\log_{10}|\alpha_0| \in [-5.6, -2.2]$, for the further calculation to avoid the inaccuracy of derivatives at boundaries (see the region between the two red lines in Fig. 2). The boundary value $\alpha_0 \approx 10^{-2.5}$ is the upper limit given by the Cassini spacecraft [27], and $\beta_0 \lesssim -4.0$ corresponds to values where spontaneous scalarization happens in the DEF theory. As a result, we have $N'_{\alpha_0} \times N_{\beta_0} = 57 \times 101 = 5757$ available nodes for constructing ROMs.

We have to point out that in practice it is difficult to calculate k_A when the scalar field is weak. In this case, a change in I_A due to the weak scalar field is comparable to the random noises induced by shooting method in solving the mTOV equations. Therefore, it is hard to keep the calculation of k_A accuracy. Here we adopt an approximation that $k_A \propto \alpha_0$ when the spontaneous scalarization is not excited [26]. Under this assumption, for a fixed β_0, we have $k_A \propto \varphi_0$ and $(\ln I_A - \ln I_A^{\rm GR}) \propto \varphi_0^2$. Thus, we choose a slightly large differential step and calculate

$$k_A = -2\varphi_0 \frac{\ln I_A^{(2)} - \ln I_A^{(1)}}{\left(\varphi_0^{(2)}\right)^2 - \left(\varphi_0^{(1)}\right)^2}, \tag{18}$$

to reduce the influence of numerical noises. In addition, there are some unexpected glitches in the results of derivatives. We remove these glitches and perform interpolation with the nearby values instead.

B. Constructing ROMs for the DEF theory

To overcome the general time-consuming computation of the mTOV integration with the shooting method, we build ROMs for the DEF theory to improve the efficiency [36, 50]. In brief, to generate a ROM for a curve $h(t; \boldsymbol{\lambda})$ with parameters $\boldsymbol{\lambda}$, one provides a training space of data $\mathbf{V} \equiv \{h(t; \boldsymbol{\lambda}_i)\}$ on a given grid of parameters. In this space, one can define a "special" inner product $\langle h(\cdot; \boldsymbol{\lambda}), h(\cdot; \boldsymbol{\lambda})\rangle$ with an inherited norm $\|h(\cdot; \boldsymbol{\lambda})\| \equiv \langle h(\cdot; \boldsymbol{\lambda}), h(\cdot; \boldsymbol{\lambda})\rangle$. Then one selects a certain number (denoted as m) of basis as a chosen space $\mathbf{RV} = \{e_i\}_{i=1}^m$ with the reduced basis (RB) method. In practice, given the starting RB ($i = 0$), one iteratively seeks for m orthonormal RBs by iterating the Gram-Schmidt orthogonalization algorithm with greedy selection to minimize the maximum projection error,

$$\sigma_i \equiv \max_{h \in \mathbf{V}} \|h(\cdot; \boldsymbol{\lambda}) - \mathcal{P}_i h(\cdot; \boldsymbol{\lambda})\|^2, \tag{19}$$

where $\mathcal{P}$ describes the projection of $h(t; \boldsymbol{\lambda})$ onto the span of the first i RBs. The process terminates when $\sigma_{m-1} \lesssim \Sigma$, a user-specified error bound. Then every curve in the training space is well approximated by

$$h(t; \boldsymbol{\lambda}) \approx \sum_{i=1}^{m} c_i(\boldsymbol{\lambda}) e_i(t) \equiv \sum_{i=1}^{m} \langle h(\cdot; \boldsymbol{\lambda}), e_i(\cdot)\rangle e_i(t), \tag{20}$$

where $c_i(\boldsymbol{\lambda})$ is the coefficient to be used for the ROM. After the RBs are built, one selects m samples $\{t_i\}_{i=1}^m$ as empirical nodes with empirical interpolation method [51]. Finally, at each empirical node, one performs a fit to the parameter space, $\{\boldsymbol{\lambda}_i\}$, and completes the construction of ROM. More details can be found in Ref. [36].

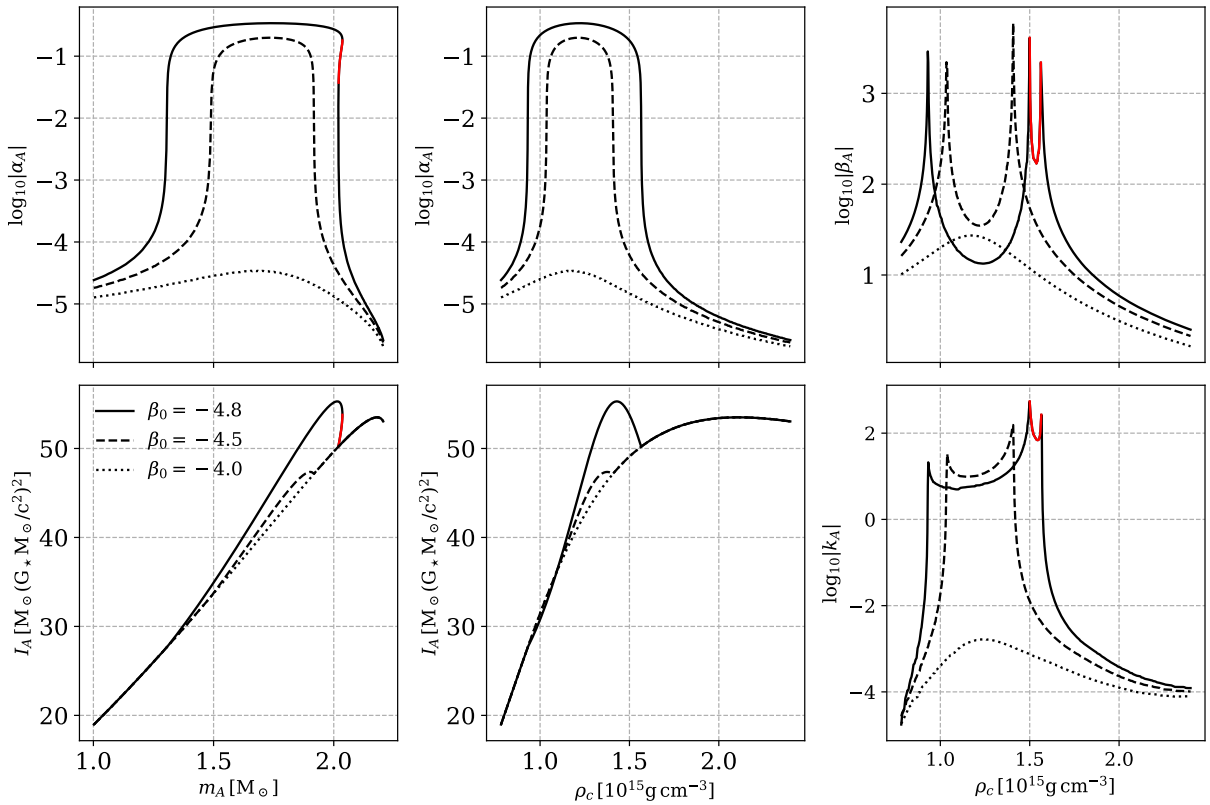

FIG. 3. Illustration of spontaneous scalarization in the DEF gravity and the numerically pathological phenomena that occur when integrating the mTOV equations for the EOS AP4. The calculation assumes DEF theories with $\log_{10}|\alpha_0| = -5.3$ and $\beta_0 = -4.8$ (solid lines), -4.5 (dashed lines) and -4.0 (dotted lines). For $\log_{10}|\alpha_0| = -5.3$, the scalar field is weak for $\beta_0 = -4.0$, strong for $\beta_0 = -4.5$, and this causes remarkable pathological phenomena for $\beta_0 = -4.8$. The red lines mark the pathological region. In this region, β_A and k_A are positive, instead of negative values as in most cases.

Extending the work of Zhao *et al.* [36], we build ROMs for six parameters, R, m_A, I_A, α_A, β_A, and k_A, as functions of the central matter density ρ_c, with specialized parameters $\boldsymbol{\lambda} = (\alpha_0, \beta_0)$. We choose the implicit parameter ρ_c as an independent variable to avoid the multivalued relations between m_A and R, as well as α_A and I_A [36]. In Fig. 3, we show the relations of the parameters and illustrate the multivalued phenomena. When $\beta_0 \lesssim -4.6$, the α_A-m_A and I_A-m_A curves are bent backwards, leading to multiple values of α_A and I_A for a given m_A. This region is marked in red in Fig. 3. The multivalued relations vanish when we use the central matter density ρ_c as an independent variable. In the red region, β_A and k_A are not negative as normal, but rather positive due to the multivalued relations. Values of α_A, β_A, and k_A span several orders of magnitude. In practice, we use $\ln|I_A|$, $\ln|\alpha_A|$, $\ln|\beta_A|$, and $\ln|k_0 - k_A|$, instead of I_A, α_A, β_A, and k_A, for a better numerical performance, where k_0 is an EOS-dependent constant set by hand to avoid negative values of $-k_A$ in the weak scalar field regime (see Fig. 3). We have $k_0 \lesssim 0.2$ generally. The training space is set to

$$\mathbf{V} = \{(\log_{10}|\alpha_0|, \beta_0) \in [-5.3, -2.5] \times [-4.8, -4.0]\}\,, \quad (21)$$

corresponding to the region between the two red lines shown in Fig. 2. As mentioned earlier, in total we have $N'_{\alpha_0} \times N_{\beta_0} = 57 \times 101 = 5757$ available nodes for building ROMs.

To balance the computation cost and the accuracy of ROMs, we set the error bound $\Sigma = 10^{-7}$ for m_A, R, and I_A, $\Sigma = 10^{-5}$ for α_A, and $\Sigma = 10^{-4}$ for β_A and k_A. The relative projection error $\tilde{\sigma}_i \equiv \sigma_i/\sigma_0$ as a function of the basis size is shown in Fig. 4. To achieve the desired projection error, the basis size is $\sim$ 20–40 for m_A, R, and I_A, but $\sim$ 150–200 for α_A, β_A, and k_A. It means that more RBs are essential to keep the accuracy of α_A, β_A, and k_A. Note that the training space contains $\sim$ 6000 curves. It implies that, to achieve a certain precision (as given by our Σ's), the curves may exhibit redundancy in the parameter space, i.e., the amount of information necessary to characterize the relations in the DEF theory to a certain desired precision is smaller than anticipated. Our ROM extracts $\sim$ 1% of the data but captures the essential information and retains the original predictions of the DEF theory to sufficient precision. The precision loss in ROM building is negligible, considering the tolerable error ($\sim$ 1%) involved in the shooting method and the calculation of derivatives. This is also verified in assessing the accuracy of the ROMs below. Eventually we perform the fits and complete the construction of the six ROMs (i.e., for R, m_A, I_A, α_A, β_A, and k_A) for each of the 15 EOSs. We encapsulate those six ROMs for the DEF theory in the `pySTGROMX` package for community use.

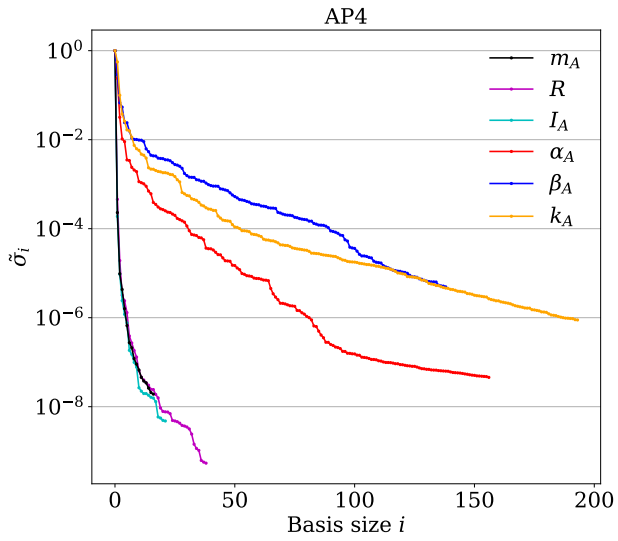

FIG. 4. Relative maximum projection errors, $\tilde{\sigma}_i$, in building the ROMs for the EOS AP4. We set $\Sigma = 10^{-7}$ for m_A, R, and I_A, $\Sigma = 10^{-5}$ for α_A, and $\Sigma = 10^{-4}$ for β_A and k_A. The $\tilde{\sigma}_i$'s of m_A, R and I_A decrease rapidly to 10^{-8} with a basis size of $\sim$ 30. On the contrary, the errors decline slowly for the coupling parameters α_A, β_A, and k_A with roughly 100–200 of basis size.

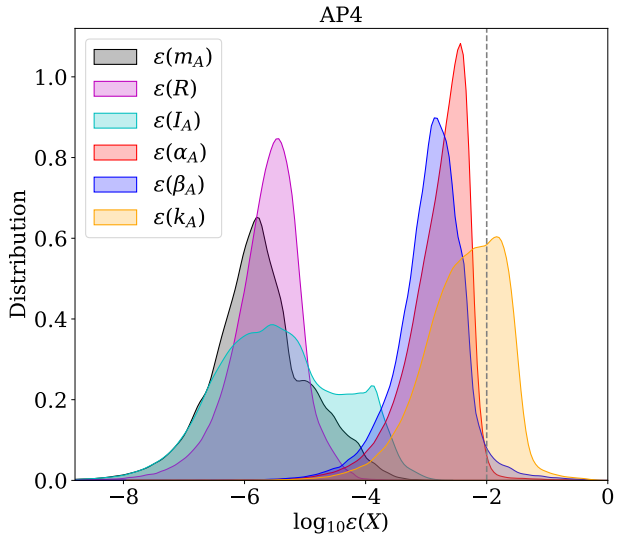

FIG. 5. Kernel density estimation (KDE) distribution of the relative error $\varepsilon(X)$, where $X \in \{m_A, R, I_A, \alpha_A, \beta_A, k_A\}$. The dashed line shows the relative tolerable error in the mTOV integration ($\lesssim$ 1%). The relative errors are small ($\lesssim 10^{-4}$) for m_A, R, and I_A but relatively large ($\lesssim 10^{-2}$) for the coupling parameters α_A, β_A, and k_A. But the errors are negligible in most practical cases.

We test the performance of the ROMs with randomly generated parameter sets $(\alpha_0, \beta_0, \rho_c)$ on our `Intel Xeon E5-2697A V4` computers. We find that the averaged time for generating the parameters improves from $\sim$ 1 second by solving the mTOV equations to $\sim$ 1 millisecond (for m_A, R, and I_A) and $\sim$ 3 milliseconds (for α_A, β_A, and k_A) by linear algebraic operations in the ROMs. Note that traditionally calculating β_A and k_A involves applying shooting method for both φ_0 and $\bar{m}_A$. The time is usually tens of seconds for generating one point in such calculation. Thus, our method improves the speed of calculating β_A and k_A by at least three orders of magnitude.

To assess the accuracy of the ROMs, we define

$$\varepsilon(X) = \left| \frac{X_{\rm ROM} - X_{\rm mTOV}}{X_{\rm ROM} + X_{\rm mTOV}} \right| , \tag{22}$$

where $X \in \{m_A, R, I_A, \alpha_A, \beta_A, k_A\}$, to indicate the fractional accuracy of the ROMs. In Eq. (22), we denote $X_{\rm ROM}$ as the prediction of ROM, and $X_{\rm mTOV}$ as the value from solving the mTOV equations with the shooting algorithm. The values $X_{\rm mTOV}$ in the test space should also be calculated at different samples but with the same method to avoid the extra error induced by the use of different methods. Thus, instead of randomly generating parameters, we set another grid as the test space which is shifted from the training space for α_0, β_0, and ρ_c, and calculate the parameters in the same way. The test space has the sparser distribution of β_0. Note that in this method we include all errors for our ROMs, including the *interpolating* errors.

The distributions of $\varepsilon(X)$ are shown in Fig. 5. The relative errors of m_A, R, and I_A are $\lesssim 10^{-5}$. On the contrary, relative errors of α_A, β_A, and k_A are mostly smaller than 1%. Although their errors are larger than those of R, m_A, and I_A, the errors are, in most cases, still small enough to be neglected compared with the numerical errors from the shooting method. For k_A, in some cases the change of I_A is rather small, as we have mentioned in Sec. III A, leading to a relatively large numerical error when calculating the derivatives. Thus, a small fraction of prediction for k_A in our ROM has a seemingly large error in the range $\sim$ 1–10%. However, we find that in such case we have $k_A \ll 1$, thus the deviation in this region has little influence on our study and will not have a practical effect.

IV. CONSTRAINTS FROM BINARY PULSARS

Constraints on the DEF parameters, α_0 and β_0, have been investigated from various gravitational systems. In the Solar System, the Cassini mission [27] gives a limit on α_0, $|\alpha_0| < 3.4 \times 10^{-3}$ at 68% confidence level (CL), from the measurement of Shapiro delay in the weak-field regime. In the strong-field regime, timing of binary pulsars provides the most stringent constraints so far to the DEF theory [26, 28, 31, 52, 57]. Here we extend the analysis in Refs. [28, 36], by carefully selecting more systems and constraining the DEF parameters in a numerically faster and reliable way with the ROMs we built in Sec. III. We will employ the MCMC technique [28, 65] to derive constraints when combining the timing observations from binary pulsar systems, including NS-WD and NS-NS systems. We will also discuss the improvements on deriving NS properties and the constraints on the DEF parameters.

TABLE I. Binary parameters of the five NS-WD systems that we use to constrain the DEF theory (PSRs J0348+0432 [52], J1012+5307 [53–56], J1738+0333 [57], J1909−3744 [58], and J2222−0137 [59]). The intrinsic time derivatives of the orbit period, $\dot{P}_b^{\rm int}$, are derived from $\dot{P}_b^{\rm obs}$ by subtracting the acceleration effect [60] and other kinematic effects such as the "Shklovskii" effect [61]. The Galactic acceleration effect is obtained from the latest Galactic potential model in Ref. [62]. For PSRs J0348+0432, J1012+5307, and J1738+0333, the pulsar masses, $m_A^{\rm obs}$, are obtained from the companion masses, $m_B^{\rm obs}$, and mass ratios, q. For PSRs J1909−3744 and J2222−0137, the masses are calculated from the Shapiro delay [28]. We list the standard 1-σ errors in units of the least significant digit(s) in parentheses.

Name	J0348+0432	J1012+5307	J1738+0333	J1909−3744	J2222−0137
Orbital period, P_b (d)	0.102424062722(7)	0.60467271355(3)	0.3547907398724(13)	1.533449474305(5)	2.44576454(18)
Eccentricity, e	0.0000026(9)	0.0000012(3)	0.00000034(11)	0.000000115(7)	0.00038096(4)
Observed $\dot{P}_b$, $\dot{P}_b^{\rm obs}$ (fs s^{-1})	−273(45)	50(14)	−17.0(31)	−510.87(13)	200(90)
Intrinsic $\dot{P}_b$, $\dot{P}_b^{\rm int}$ (fs s^{-1})	−274(45)	−5(9)	−27.72(64)	−4.4(79)	−60(90)
Periastron advance, $\dot{\omega}$ (deg yr^{-1})	—	—	—	—	0.1001(35)
Einstein delay γ (ms)	—	—	—	—	—
Pulsar mass, $m_A^{\rm obs}$ ($M_\odot$)	—	—	—	1.492(14)	1.76(6)
Companion mass, $m_B^{\rm obs}$ ($M_\odot$)	$0.1715^{+0.0045}_{-0.0030}$	0.174(7)	$0.1817^{+0.0073}_{-0.0054}$	0.209(1)	1.293(25)
Mass ratio, $q \equiv m_A/m_B$	11.70(13)	10.5(5)	8.1(2)	—	—

TABLE II. Binary parameters of the three NS-NS systems that we use to constrain the DEF theory (PSRs B1913+16 [63], J0737−3039A [48], and J1757−1854 [64]). For PSR B1913+16, the masses are determined from measurement of periastron advance, $\dot{\omega}$, and Einstein delay, γ. For PSR J0737−3039A, the masses are determined from the measurement of $\dot{\omega}$ and theory-independent mass ratio q. For PSR J1757−1854, the masses are derived from DDGR model. Similar to Table I, we list the standard 1-σ errors in units of the least significant digit(s) in parentheses.

Name	B1913+16	J0737−3039A	J1757−1854
Orbital period, P_b (d)	0.322997448918(3)	0.10225156248(5)	0.18353783587(5)
Eccentricity, e	0.6171340(4)	0.0877775(9)	0.6058142(10)
Observed $\dot{P}_b$, $\dot{P}_b^{\rm obs}$ (fs s^{-1})	−2423(1)	−1252(17)	−5300(200)
Intrinsic $\dot{P}_b$, $\dot{P}_b^{\rm int}$ (fs s^{-1})	−2398(4)	−1252(17)	−5300(240)
Periastron advance, $\dot{\omega}$ (deg yr^{-1})	4.226585(4)	16.89947(68)	10.3651(2)
Einstein delay γ (ms)	4.307(4)	0.3856(26)	3.587(12)
Pulsar mass, $m_A^{\rm obs}$ ($M_\odot$)	1.438(1)	1.3381(7)	1.3384(9)
Companion mass, $m_B^{\rm obs}$ ($M_\odot$)	1.390(1)	1.2489(7)	1.3946(9)
Mass ratio, $q \equiv m_A/m_B$	—	1.0714(11)	—

A. Setup

Previous work [28, 36] has constrained the spontaneous scalarization of the DEF theory via MCMC simulations by combining some well-timed binary pulsars. These previous studies considered five well-timed NS-WD binary pulsars, PSRs J0348+0432 [52], J1012+5307 [53–56], J1738+0333 [57], J1909−3744 [58], and J2222−0137 [59]. We include these five systems in our study as well and their latest relevant parameters are listed in Table I. For these systems, WD companions are weakly self-gravitating objects, leading to a tiny effective scalar coupling $\alpha_B \approx \alpha_0$. It indicates a large dipolar contribution $\propto (\alpha_A - \alpha_0)^2$ to $\dot{P}_b$, if α_A is sufficiently different from α_0 [see Eq. (8)]. As explained in the caption of Table I, the measurements of the masses are independent of the PPK parameter $\dot{P}_b$. Thus, we can safely place bounds on the parameters of the DEF theory by utilizing these masses and the intrinsic orbital decay rate, $\dot{P}_b^{\rm int}$.

Apart from the five NS-WD systems, we add three NS-NS systems in our study. As discussed above, due to the closeness of α_A and α_B, the dipolar radiation of these (almost) symmetric double NS systems is small, making it difficult to constrain the DEF theory with $\dot{P}_b$. However, as shown in Sec. II, some other PPK parameters derived from pulsar timing, such as the periastron advance rate $\dot{\omega}$ and the Einstein delay parameter γ, are also modified in the DEF theory. These modifications are considerable, especially for NS-NS binaries. Therefore, these double NS systems are potentially powerful laboratories to constrain the free parameters of the DEF theory. In Table II, we show parameters of three well-timed double NSs used in this study: PSRs B1913+16 [63], J0737−3039A [48], and J1757−1854 [64]. In these systems, the measurements of the masses depend on PPK parameters. For PSR B1913+16, the masses are determined from measurement of periastron advance, $\dot{\omega}$, and Einstein delay, γ. For PSR J0737−3039, the masses are determined from the measurement of $\dot{\omega}$ and theory-independent mass ratio q. For PSR J1757−1854, the masses are determined from the DDGR model [66, 67], which includes the contribution from all PPK parameters via their GR formats. In principle, only the independent subset of PPK parameters that were not used in deriving masses can be utilized to constrain the DEF parameters.

To obtain NSs' properties, we need to assume a particular EOS. In this study, as mentioned earlier, we adopt 15 EOSs, namely AP3, AP4, BL_EOS, BSk20, BSk21, BSk22, BSk25, ENG, MPA1, PAL1, SLy4, SLy9, SLy230a, WFF1, and WFF2 (see Ref. [68] for a review). The mass-radius relations from these EOSs are shown in Fig. 1. These EOSs are

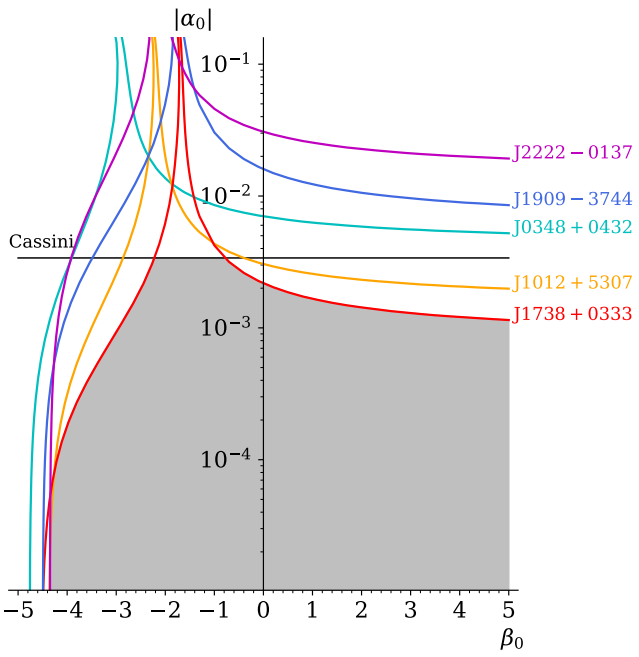

FIG. 6. Constraints on the DEF parameters (α_0, β_0) from a variety of binary pulsars on the DEF theory with the EOS AP4. Regions above curves are excluded, and the shaded area is the region that passes all tests in this plot. "Cassini" stands for the upper limit from the Shapiro time-delay measurement in the Solar System [27].

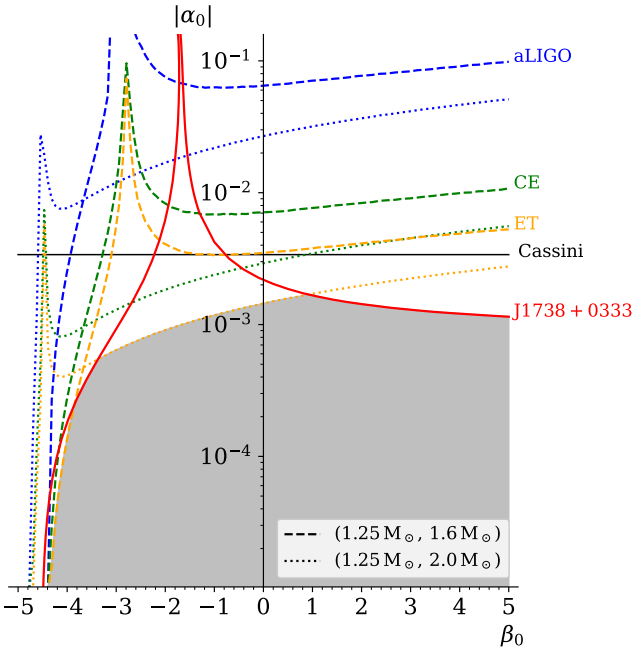

FIG. 7. Similar to Fig. 6, but with *projected* limits from aLIGO, CE and ET with hypothetical GW signals of BNSs at a distance of 200 Mpc. The dashed lines represent the constraints from a (1.25 $M_\odot$, 1.6 $M_\odot$) BNS merger event, and the dotted lines correspond to a (1.25 $M_\odot$, 2.0 $M_\odot$) event. The shaded area is an illustration for combining all these constraints. We plot the limits from PSR J1738+0333 and the Cassini mission for comparison.

all consistent with the observed 2 $M_\odot$ maximum mass limit of NSs, and they are chosen inclined towards those which predict NS radii around ∼ 11–13 km, as favored by the tidal deformability measurement in GW170817 [11, 69].

B. Constraints from individual pulsars

Before the MCMC simulations, we can estimate the constraints on the DEF parameters, α_0 and β_0, from individual binary systems. We saturate the uncertainties on individual PPK parameters to determine the upper limits of the DEF parameters. By determining if the predicted value $\dot{P}_b^{\rm th}$ from Eqs. (8) and (9) lies within the 1-σ range of $\dot{P}_b^{\rm int}$, i.e., $\dot{P}_b^{\rm int} \pm \delta\dot{P}_b^{\rm int}$, we obtain the limits on the difference of effective scalar couplings α_A and α_B, i.e. $|\Delta\alpha| = |\alpha_A - \alpha_B|$. With it, we constrain parameters α_0 and β_0.

In Fig. 6, we show the constraints on α_0 and β_0 obtained from binary pulsars. In these systems, PSR J1738+0333 gives almost the most stringent constraint. The upper limit of β_0 can reach ∼ −4.4 from PSRs J1012+5307 and J2222−0137. When β_0 is around −3 to −2, the constraints from binary pulsars are weak, leading to a peak of $|\alpha_0|$. However, the limit from the Cassini mission helps exclude this region. In Fig. 7, we show constraints from hypothetical asymmetric BNS merger events at 200 Mpc, to be probed by GW detectors including Advanced LIGO (aLIGO), CE, and ET [28]. We assume two hypothetical BNSs with masses, (1.25 $M_\odot$, 1.6 $M_\odot$) and (1.25 $M_\odot$, 2.0 $M_\odot$), and the limits are obtained from Fisher information matrix [35]. It is shown that the GW detectors could help in constraining the DEF parameters if such BNSs are observed. Among the three detectors, ET would probably provide tighter bounds, due to its lower starting frequency. Note that these constraints are dependent on the specific EOS, and in Figs. 6 and 7 we have assumed EOS AP4. The results are similar to previous results in Refs. [28, 57].

C. The Bayesian inference and the MCMC framework

We here explore the constraints on the DEF theory combining the well-timed binary pulsars through MCMC simulations. MCMC technique provides a convenient and statistically sound algorithm to generate the distribution of unknown parameters for a model with many free parameters. In this study, we use `EMCEE`,[3] a python implementation of an affine-invariant MCMC ensemble sampler, and our `pySTGROMX` package to speed up the calculation within the Bayesian framework.

In the Bayesian inference, given priors, hypothesis $\mathcal{H}$, data $\mathcal{D}$, and all the extra relevant information $\mathcal{I}$, the posterior distribution of the DEF parameters (α_0, β_0), $P(\alpha_0, \beta_0|\mathcal{D}, \mathcal{H}, \mathcal{I})$,

[3] https://github.com/dfm/emcee

can be inferred by

$$P(\alpha_0,\beta_0|\mathcal{D},\mathcal{H},\mathcal{I}) = \int \frac{P(\mathcal{D}|\alpha_0,\beta_0,\Xi,\mathcal{H},\mathcal{I})P(\alpha_0,\beta_0,\Xi|\mathcal{H},\mathcal{I})}{P(\mathcal{D}|\mathcal{H},\mathcal{I})}\mathrm{d}\Xi\,, \tag{23}$$

where Ξ denotes all the other unknown parameters in the theory. In Eq. (23), $P(\mathcal{D}|\alpha_0,\beta_0,\Xi,\mathcal{H},\mathcal{I})$ is the likelihood function, $P(\alpha_0,\beta_0,\Xi|\mathcal{H},\mathcal{I})$ the prior, and

$$P(\mathcal{D}|\mathcal{H},\mathcal{I}) = \int P(\mathcal{D}|\Xi,\mathcal{H},\mathcal{I})P(\Xi|\mathcal{H},\mathcal{I})\mathrm{d}\Xi\,, \tag{24}$$

the *model evidence* which merely plays a role of normalization here [70]. Based on Eq. (23), MCMC method generates a sampling of values (α_0, β_0) that satisfies the posterior distribution.

In the MCMC simulations, the parameters, α_0 and β_0, are constrained by evaluating the likelihood function. Considering all the binary pulsar systems we include, we use a general logarithmic likelihood function,

$$\ln\mathcal{L}_{\rm PSR} = -\frac{1}{2}\sum_{i=1}^{N_{\rm PSR}}\left[\left(\frac{\dot{P}_b-\dot{P}_b^{\rm int}}{\sigma_{\dot{P}_b^{\rm int}}}\right)^2+\left(\frac{\dot{\omega}-\dot{\omega}^{\rm obs}}{\sigma_{\dot{\omega}^{\rm obs}}}\right)^2+\left(\frac{\gamma-\gamma^{\rm obs}}{\sigma_{\gamma^{\rm obs}}}\right)^2 + \left(\frac{m_A-m_A^{\rm obs}}{\sigma_{m_A^{\rm obs}}}\right)^2+\left(\frac{m_B-m_B^{\rm obs}}{\sigma_{m_B^{\rm obs}}}\right)^2\right]_i, \tag{25}$$

for $N_{\rm PSR}$ binary pulsars. Here we assume that observations of different binary pulsars are independent. The intrinsic orbital decay $\dot{P}_b^{\rm int}$, the periastron advance rate $\dot{\omega}^{\rm obs}$, the Einstein delay parameter $\gamma^{\rm obs}$, the pulsar mass $m_A^{\rm obs}$, and the companion mass $m_B^{\rm obs}$ are given in Tables I and II. The 1-σ uncertainty, σ_X, is the observational uncertainty for parameter X, where $X \in \left\{\dot{P}_b^{\rm int},\dot{\omega}^{\rm obs},\gamma^{\rm obs},m_A^{\rm obs},m_B^{\rm obs}\right\}$. The parameters, $\dot{P}_b$, $\dot{\omega}$, γ, and m_A are dependent on the parameter set, (α_0,β_0,Ξ). The companion mass m_B is consistently given from the parameter set (α_0,β_0,Ξ) as well when it is a NS. Otherwise, for a WD, it is picked randomly within the 1-σ uncertainty of $m_B^{\rm obs}$.

For WD companions, the coupling parameters can be reduced to $\alpha_B = \alpha_0$ and $\beta_B = \beta_0$. Thus, their contributions to $\dot{\omega}$ and γ can be neglected. In addition to the five NS-WD binary pulsars that have been investigated in Refs. [28, 36], we combine three extra double NS systems. In these NS-NS systems, we could utilize the information from $\dot{\omega}$ and γ. However, not each pulsar's measurements of $\dot{\omega}$, γ, m_A, and m_B are independent, as we have mentioned above. Thus, only for some suitable pulsar systems, the contributions of $\dot{\omega}$ and γ are counted in a consistent way. In this study, we combine the contributions from $\dot{P}_b^{\rm int}$ of eight binary pulsars and γ of PSR J0737−3039A in total for our estimation. In this way, we utilize the available information from the timing data as much as possible.

Note that the other parameters included in MCMC calculations, such as the orbital period, P_b, and the orbital eccentricity, e, are determined very well from the observations (see Tables I and II). Thus, we adopt their central values for simplicity in the process of MCMC calculations, which is sufficient in the context.

Now, we describe the details of employing the MCMC technique to get the posteriors from the priors on (α_0,β_0) and the log-likelihood function (25). In the MCMC calculation, the information we utilize to constrain the parameter space of (α_0,β_0) is from the NSs. In total, we have $N = N_{\rm NS-WD} + 2N_{\rm NS-NS}$ NSs from the observations. To describe the observational signatures fully in the DEF theory, we need $N+2$ free parameters, collectively denoted as $\boldsymbol{\theta} = \left\{\alpha_0,\,\beta_0,\,\rho_c^{(i)}\,(i=1,2,...,N)\right\}$ where $\rho_c^{(i)}$ is the central matter density of NS i in the Jordan frame. The initial values of $\rho_c^{(i)}$ are sampled around their GR values. We allow the simulation to explore a large region of central matter density. Thanks to our ROMs, the initial central values of the scalar field φ_c are no longer needed during the calculation, which avoids extra computationally intensive calculations [28]. Using α_0, β_0, and $\rho_c^{(i)}$, we obtain the properties of NSs. Then we calculate the PPK parameters and the log-likelihood functions to evaluate the posteriors.

For our studies, we carefully choose the priors of (α_0, β_0) to cover the region of interest where the spontaneous scalarization develops. For each MCMC run, we assume a uniform prior distribution of $(\log_{10}|\alpha_0|,\,\beta_0)$ in the region of our ROMs, i.e., $(\log_{10}|\alpha_0|,\,\beta_0) \in [-5.3,-2.5]\times[-4.8,-4.0]$.

For each MCMC simulation, we use 32 walkers (chains) and 100,000 steps for each walker. Thus, we produce 3.2 million samples in total. The first half chain samples are discarded as the *BURN-IN* phase [65, 71]. Then we "thin" the remaining samples, with a thinning factor of ten, to reduce the correlation of the adjacent samples. We perform the Gelman-Rubin test for convergence, and we have confirmed that our samples pass the test [71]. Thus, our posteriors of α_0 and β_0 are statistically reliable. We end up with 1.6×10^5 "thinned" samples for each simulation to infer the marginalized distributions of the free parameters α_0 and β_0. Eventually, we apply this procedure to all the 15 EOSs.

D. Constraints from combining binary pulsars

In this subsection, we show the constraints from the timing measurements of binary pulsars from the application of our ROMs. To achieve the speedups of MCMC calculations, we restrict the priors of $\log_{10}|\alpha_0|$ and β_0 to the same ranges as in our ROMs. With the MCMC simulations done, we can obtain the posterior distributions of the DEF parameters $\log_{10}|\alpha_0|$ and β_0 for the 15 EOSs we adopt.

In Fig. 8, as an example, we show the marginalized 2-dimensional (2-d) and 1-d posterior distributions in the parameter space of $(\log_{10}|\alpha_0|,\,-\beta_0)$ and the constraints at 68% and 90% CLs for EOS AP4. As mentioned above, the priors of $(\log_{10}|\alpha_0|,\,-\beta_0)$ are uniform distributions in the rectangle region of Fig. 8. The results from pulsars provide very tight constraints on the parameters of the DEF theory. The upper limits of $\log_{10}|\alpha_0|$ and $-\beta_0$ are constrained to ~ -3.9 and ~ 4.3 at 90% CL, respectively. The constraints are overall similar to previous results from Refs. [28, 36]. The extra double NS systems provide certain but not remarkable improvements in our results. The tight constraints are mainly contributed by

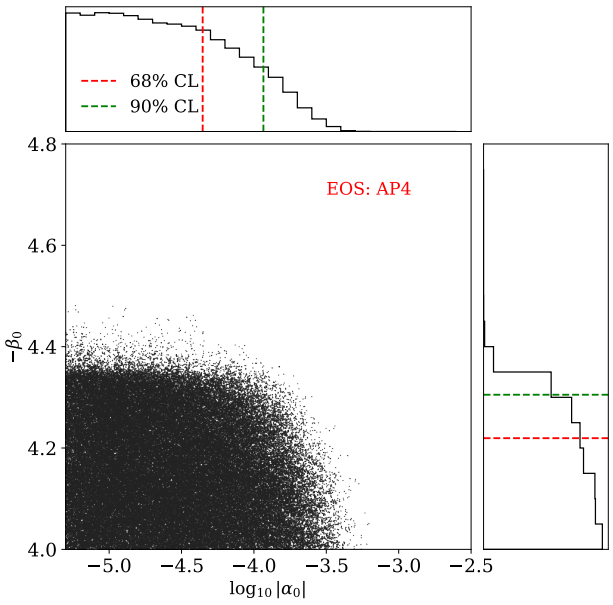

FIG. 8. The marginalized 2-d distribution in the parameter space of $(\log_{10}|\alpha_0|, -\beta_0)$ from MCMC runs on the eight pulsars listed in Tables I and II for the EOS AP4. The marginalized 1-d distributions and the corresponding upper limits at 68% CL and 90% CL are illustrated in upper and right panels.

the dipolar radiation in the NS-WD systems. Here, we mainly aim to provide a test that proves the ability of our method to constrain these parameters. In the future, with the further precise observations of binary pulsars, the PPK parameters $\dot{\omega}$ and γ might provide additional constraints for the DEF gravity.

We apply the analysis above to all the 15 EOSs. The marginalized 2-d and 1-d distributions from the MCMC results for all the 15 EOSs we include in this study are shown in Fig. 9. In addition, in Fig. 10 we show the 1-d distributions of $\log_{10}|\alpha_0|$ and $-\beta_0$, and their upper bounds at 68% and 90% CLs for all the EOSs. These results are overall similar, but show the dependence on the choice of EOS. The upper bounds on α_0 at 90% CL are approximately 10^{-4}. The upper bounds on $-\beta_0$ at 90% CL are ~ 4.3.

Using our ROMs, we can conveniently discuss the spontaneous scalarization phenomena of a NS. In Fig. 11, we illustrate the upper bounds at 90% CL on the absolute values of coupling parameters: effective scalar coupling α_A and its derivative, β_A, as well as coupling factor for the moment of inertial, k_A, as functions of the NS mass, m_A. The ranges below the curves mark the regions that are unconstrained up to now. It is shown clearly that, for all the 15 EOSs, the allowed maximum values of these parameters are constrained tightly. In left panel of Fig. 11, the upper bounds at 90% CL on the NSs show that for some EOSs, the maximal effective scalar coupling allowed is $\sim 10^{-2}$. A remarkable scalarization of NS at this level is still permitted for a NS with a suitable mass within the range of 1.6–2.0 $M_\odot$. Compared with earlier results [28, 36], the "scalarization window" is still open though slightly limited further. An improvement in this study is that, besides the scalar coupling α_A, we can investigate the coupling parameters β_A and k_A conveniently with our ROMs. As shown in the middle and right panels of Fig. 11, the peaks with extremely large values of β_A and k_A shown in Fig. 3 due to the fact of strong scalarization are essentially ruled out. Only mild deviation is permitted now. The maximum values are $\sim 3 \times 10^2$ for $|\beta_A|$ and ~ 10 for $|k_A|$. Therefore, a very large deviation of these scalar coupling parameters from GR is not expected based on the contemporary observation. However, there is still some room for a noteworthy spontaneous scalarization.

Combining the results, we note that for a stiffer EOS, spontaneous scalarization tends to be significant for larger mass, from 1.4–1.7 $M_\odot$ (EOS WFF1) to 1.8–2.2 $M_\odot$ (EOS PAL1). Most of the NS masses in our study lie in $m_A \sim 1.3$–$1.7\,M_\odot$. As a consequence, the MCMC simulation shows that, the tightest constraint is obtained for EOS WFF1.

In a short summary, we provide a quick and statistically reliable method to constrain the DEF parameters. We verify the validity of the method and give the stringent constraints on the DEF theory. The bounds are slightly improved, but overall similar to previous studies [28, 36]. Constraints on $|\alpha_0|$ and β_0 depend on the precision of the observation, choice of pulsar systems, EOSs, and priors. The "scalarization window" is still open at the level of $\sim 10^{-2}$ for all the EOSs. More observations and suitable systems in the future, such as possible observations of pulsar timing and GWs from BNSs with NS masses lying in the "scalarization window", will help to place new constraints on the DEF theory.

V. CONCLUSION

In this paper, we investigate the DEF theory that predicts large deviations from GR for NSs through nonperturbative spontaneous scalarization phenomena. We briefly review the scalarization phenomena of the DEF theory and relevant predictions. To avoid solving the mTOV equations for slowly rotating NSs repeatedly, which is time-consuming and computationally expensive, we construct efficient ROMs to derive NSs' properties including m_A, R, I_A, α_A, β_A, and k_A for the DEF theory. Based on the contemporary observations about the properties of NSs, such as masses and radii, we build ROMs for 15 carefully selected EOSs, extending earlier work. The ROMs for our calculations are coded in a python package `pySTGROMX` and made public for the community use. After testing the performance of the ROMs, we find that, compared with the shooting algorithm, our ROMs can speed up the relevant calculations by two orders of magnitude for α_A and even three orders for β_A and k_A, and yet still keep accuracy at $\sim 1\%$ level. This gives an accurate and more comprehensive description of NSs' properties in DEF gravity.

As an application, we utilize `pySTGROMX` to explore constraints on the DEF theory with well-timed binary pulsars through MCMC simulations. We use the latest precise data from five NS-WD systems and three NS-NS systems, to derive tight constraint of the DEF theory. We bound the DEF parameters to be $|\alpha_0| \lesssim 10^{-3.9}$ and $-\beta_0 \lesssim 4.3$ at the 90% CL for a variety of EOSs. The constraints are dependent on the precision of the observation, choice of pulsar systems, priors,

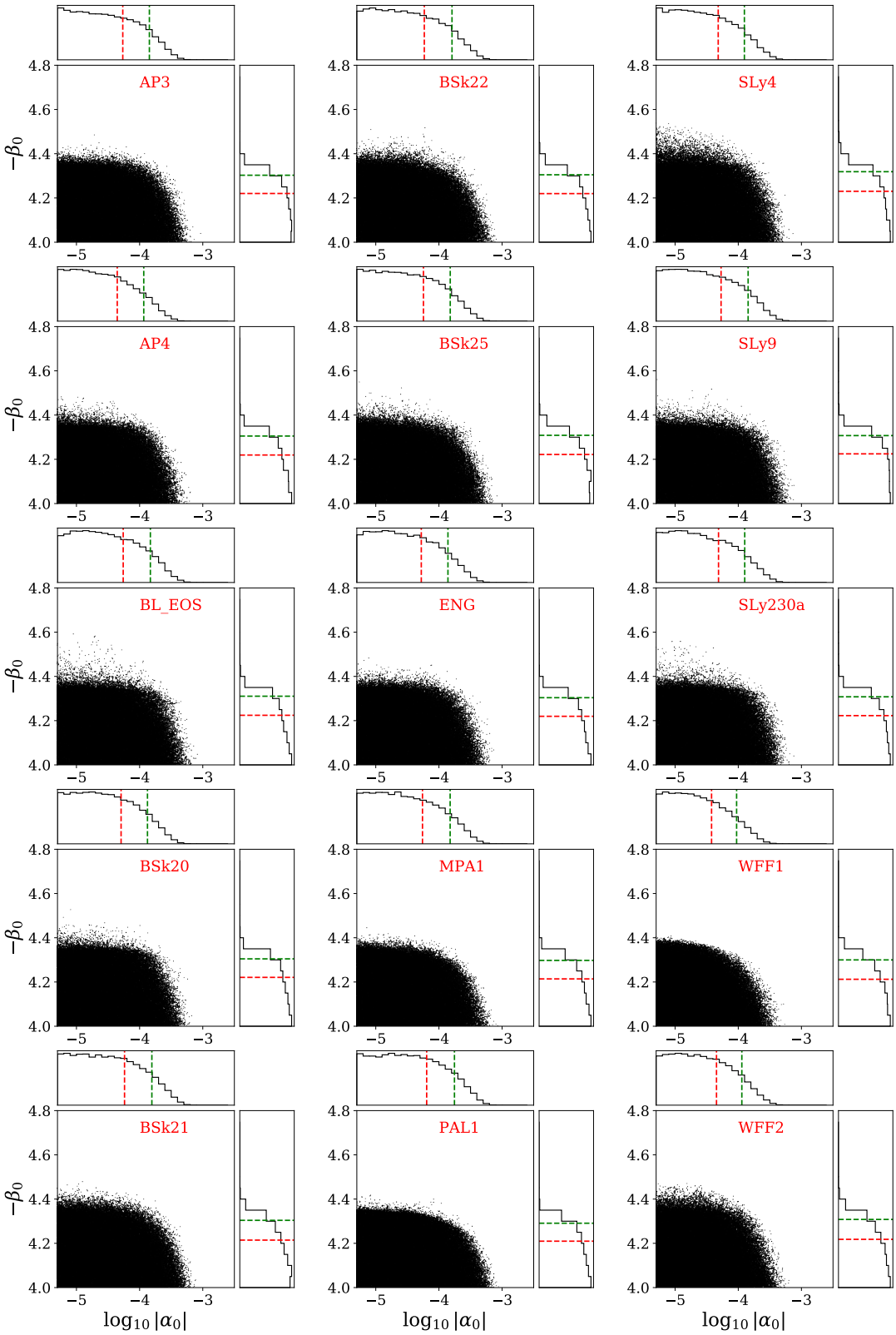

FIG. 9. The marginalized 2-d distribution in the parameter space of $(\log_{10}|\alpha_0|, -\beta_0)$ from MCMC runs on the eight pulsars listed in Tables I and II for all the 15 EOSs. The marginalized 1-d distributions and the upper limits at 68% CL and 90% CL are illustrated in upper and right subpanels of each panel.

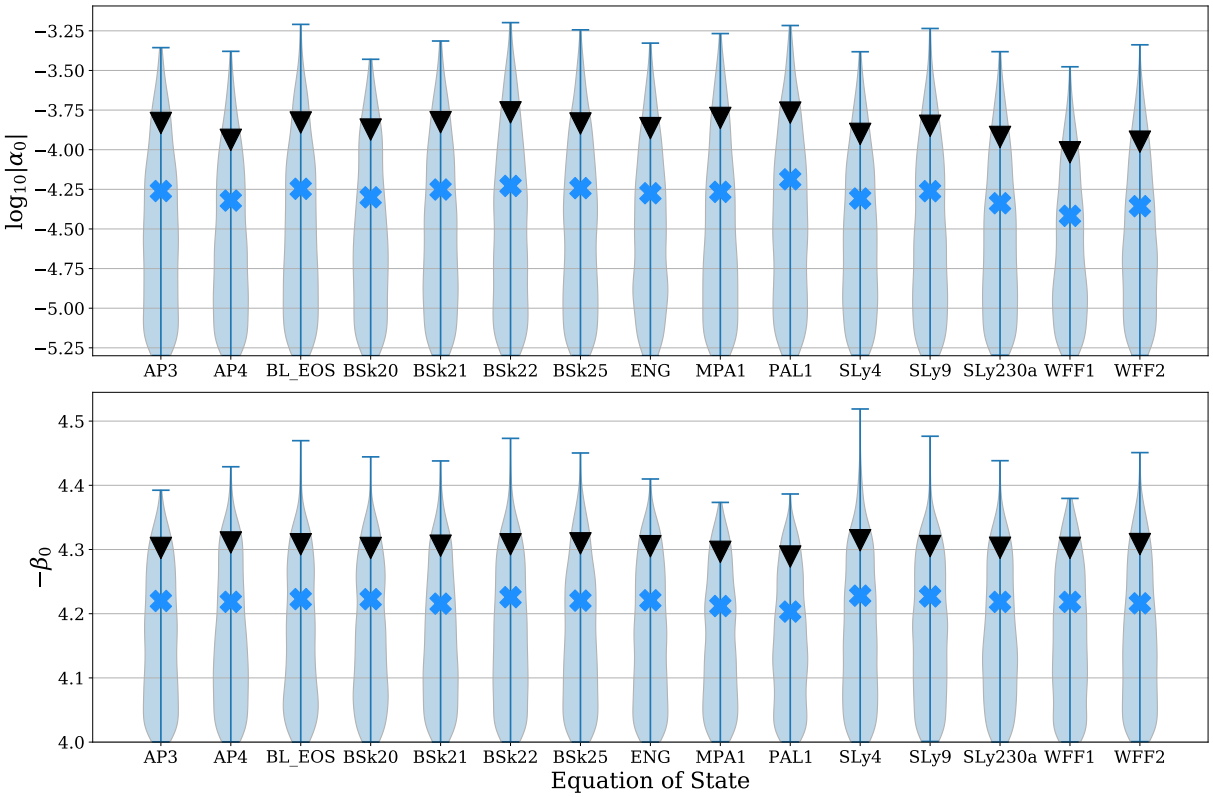

FIG. 10. Violin plots of the marginalized 1-d posterior distributions in the parameter space of $\log_{10}|\alpha_0|$ (upper panel) and $-\beta_0$ (lower panel) for 15 EOSs in our study. The 90% and 68% CL upper bounds are shown by the black and blue markers, respectively.

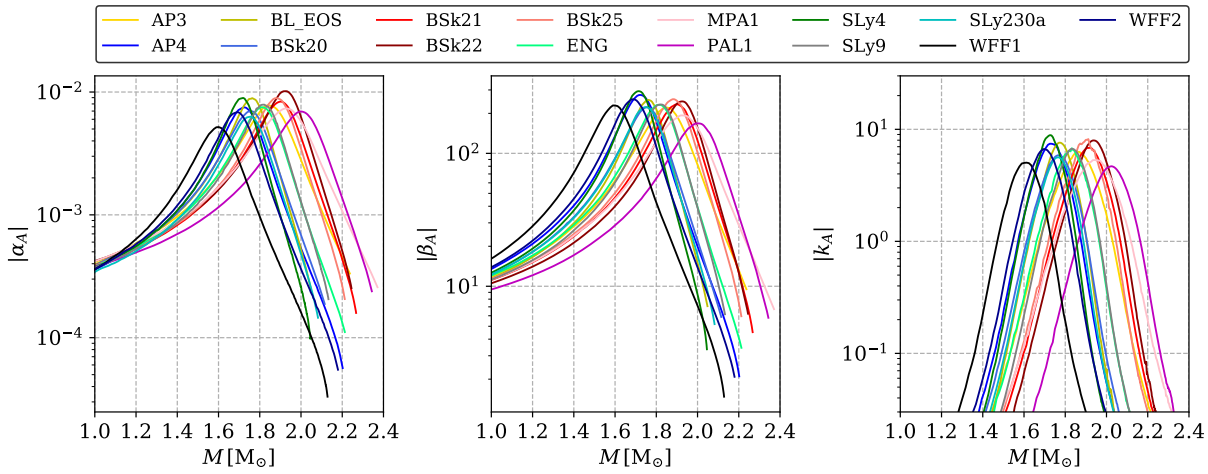

FIG. 11. The upper bounds at 90% CL on the NS effective scalar coupling parameters, α_A, β_A, and k_A, considering the combined constraints from the five NS-WD pulsars in Table I and three NS-NS pulsars in Table II.

and EOSs. We find that the "scalarization window" still exists at $\sim 10^{-2}$ level. In the future, if NSs whose masses lie around the "scalarization window" can be observed precisely, the possibility of a strong scalarization for NSs may be excluded entirely.

In the future, the new large radio telescopes, e.g., the Five-hundred-meter Aperture Spherical radio Telescope (FAST) in China [72] and the Square Kilometre Array (SKA) in Australia and South Africa [73, 74], are expected to improve the precision of pulsar timing and also discover new pulsar systems. These would help to close the "scalarization window". Furthermore, the current and next-generation GW detectors, such as the aLIGO, CE, ET, and KAGRA, could have more detection of compact binary coalescences in the future. These

observations would provide more information to be used to investigate alternative theories of gravity in a more precise and accurate way. Our ROMs are constructed to satisfy the requirements of quick evaluation of the parameters in the DEF theory, suitable for applications for binary pulsar experiments, as well as GWs to some extent.

ACKNOWLEDGMENTS

We are grateful to Norbert Wex for helpful discussions. This work was supported by the National SKA Program of China (2020SKA0120300), the National Natural Science Foundation of China (11975027, 11991053, 11721303), the Young Elite Scientists Sponsorship Program by the China Association for Science and Technology (2018QNRC001), the Max Planck Partner Group Program funded by the Max Planck Society, and the High-performance Computing Platform of Peking University.

[1] A. Einstein, Sitzungsber. Preuss. Akad. Wiss. Berlin (Math. Phys.) **1915**, 844 (1915).
[2] C. M. Will, Living Reviews in Relativity **17**, 4 (2014), arXiv:1403.7377 [gr-qc].
[3] T. Clifton, P. G. Ferreira, A. Padilla, and C. Skordis, Phys. Rept. **513**, 1 (2012), arXiv:1106.2476 [astro-ph.CO].
[4] I. H. Stairs, Living Reviews in Relativity **6**, 5 (2003), arXiv:astro-ph/0307536 [astro-ph].
[5] N. Wex, in *Frontiers in Relativistic Celestial Mechanics: Applications and Experiments*, Vol. 2, edited by S. M. Kopeikin (Walter de Gruyter GmbH, Berlin, Boston, 2014) p. 35, arXiv:1402.5594 [gr-qc].
[6] L. Shao and N. Wex, Sci. China Phys. Mech. Astron. **59**, 699501 (2016), arXiv:1604.03662 [gr-qc].
[7] B. Abbott *et al.* (LIGO Scientific and Virgo Collaborations), Phys. Rev. Lett. **116**, 221101 (2016), [Erratum: Phys.Rev.Lett. 121, 129902 (2018)], arXiv:1602.03841 [gr-qc].
[8] B. P. Abbott *et al.* (LIGO Scientific and Virgo Collaborations), Phys. Rev. Lett. **118**, 221101 (2017), [Erratum: Phys.Rev.Lett. 121, 129901 (2018)], arXiv:1706.01812 [gr-qc].
[9] B. Abbott *et al.* (LIGO Scientific and Virgo Collaborations), Phys. Rev. D **100**, 104036 (2019), arXiv:1903.04467 [gr-qc].
[10] R. Abbott *et al.* (LIGO Scientific and Virgo Collaborations), (2020), arXiv:2010.14529 [gr-qc].
[11] B. Abbott *et al.* (LIGO Scientific and Virgo Collaborations), Phys. Rev. Lett. **119**, 161101 (2017), arXiv:1710.05832 [gr-qc].
[12] B. P. Abbott *et al.*, Astrophys. J. Lett. **848**, L12 (2017), arXiv:1710.05833 [astro-ph.HE].
[13] B. Abbott *et al.* (LIGO Scientific and Virgo Collaborations), Phys. Rev. Lett. **123**, 011102 (2019), arXiv:1811.00364 [gr-qc].
[14] E. Berti *et al.*, Class. Quant. Grav. **32**, 243001 (2015), arXiv:1501.07274 [gr-qc].
[15] C. M. Will, *Theory and Experiment in Gravitational Physics* (Cambridge University Press, Cambridge, England, 2018).
[16] T. Kaluza, Int. J. Mod. Phys. D **27**, 1870001 (2018), arXiv:1803.08616 [physics.hist-ph].
[17] O. Klein, Zeitschrift fur Physik **37**, 895 (1926).
[18] Y. Fujii and K. Maeda, *The Scalar-tensor Theory of Gravitation*, Cambridge Monographs on Mathematical Physics (Cambridge University Press, Cambridge, England, 2007).
[19] H. Goenner, Gen. Rel. Grav. **44**, 2077 (2012), arXiv:1204.3455 [gr-qc].
[20] P. Jordan, Nature **164**, 637 (1949).
[21] P. Jordan, Z. Phys. **157**, 112 (1959).
[22] M. Fierz, Helv. Phys. Acta **29**, 128 (1956).
[23] C. Brans and R. Dicke, Phys. Rev. **124**, 925 (1961).
[24] T. Damour and G. Esposito-Farèse, Classical and Quantum Gravity **9**, 2093 (1992).
[25] T. Damour and G. Esposito-Farèse, Phys. Rev. Lett. **70**, 2220 (1993).
[26] T. Damour and G. Esposito-Farèse, Phys. Rev. D **54**, 1474 (1996).
[27] B. Bertotti, L. Iess, and P. Tortora, Nature **425**, 374 (2003).
[28] L. Shao, N. Sennett, A. Buonanno, M. Kramer, and N. Wex, Physical Review X **7**, 041025 (2017), arXiv:1704.07561 [gr-qc].
[29] N. Sennett, L. Shao, and J. Steinhoff, Phys. Rev. D **96**, 084019 (2017), arXiv:1708.08285 [gr-qc].
[30] T. Damour, in *Physics of Relativistic Objects in Compact Binaries: From Birth to Coalescence*, Vol. 359, edited by M. Colpi, P. Casella, V. Gorini, U. Moschella, and A. Possenti (Springer, Dordrecht, 2009) p. 1, arXiv:0704.0749 [gr-qc].
[31] D. Anderson, P. Freire, and N. Yunes, Class. Quant. Grav. **36**, 225009 (2019), arXiv:1901.00938 [gr-qc].
[32] L. Shao, in *8th Meeting on CPT and Lorentz Symmetry* (2019) arXiv:1905.08405 [gr-qc].
[33] T. Damour and J. H. Taylor, Phys. Rev. D **45**, 1840 (1992).
[34] R. Abbott *et al.* (LIGO Scientific and Virgo Collaborations), (2020), arXiv:2010.14527 [gr-qc].
[35] L. S. Finn, Phys. Rev. **D46**, 5236 (1992), arXiv:gr-qc/9209010 [gr-qc].
[36] J. Zhao, L. Shao, Z. Cao, and B.-Q. Ma, Phys. Rev. D **100**, 064034 (2019).
[37] B. P. Abbott *et al.* (LIGO Scientific Collaboration), Class. Quant. Grav. **34**, 044001 (2017), arXiv:1607.08697 [astro-ph.IM].
[38] S. Hild *et al.*, Class. Quant. Grav. **28**, 094013 (2011), arXiv:1012.0908 [gr-qc].
[39] K. Yagi and T. Tanaka, Prog. Theor. Phys. **123**, 1069 (2010), arXiv:0908.3283 [gr-qc].
[40] M. A. Sedda *et al.*, Class. Quant. Grav. **37**, 215011 (2020), arXiv:1908.11375 [gr-qc].
[41] M. Arca Sedda *et al.*, Exp. Astron. (2021), 10.1007/s10686-021-09713-z, arXiv:2104.14583 [gr-qc].
[42] C. Liu, L. Shao, J. Zhao, and Y. Gao, Mon. Not. Roy. Astron. Soc. **496**, 182 (2020), arXiv:2004.12096 [astro-ph.HE].
[43] J. M. Lattimer and M. Prakash, Astrophys. J. **550**, 426 (2001), arXiv:astro-ph/0002232 [astro-ph].
[44] L. Shao, AIP Conf. Proc. **2127**, 020016 (2019), arXiv:1901.07546 [gr-qc].
[45] F. M. Ramazanoğlu and F. Pretorius, Phys. Rev. D **93**, 064005 (2016), arXiv:1601.07475 [gr-qc].

[46] R. Xu, Y. Gao, and L. Shao, Phys. Rev. D **102**, 064057 (2020), arXiv:2007.10080 [gr-qc].

[47] E. Barausse, C. Palenzuela, M. Ponce, and L. Lehner, Phys. Rev. D **87**, 081506 (2013).

[48] M. Kramer *et al.*, Science **314**, 97 (2006), arXiv:astro-ph/0609417.

[49] E. Fonseca *et al.*, (2021), arXiv:2104.00880 [astro-ph.HE].

[50] S. E. Field, C. R. Galley, J. S. Hesthaven, J. Kaye, and M. Tiglio, Phys. Rev. X **4**, 031006 (2014), arXiv:1308.3565 [gr-qc].

[51] M. Barrault, Y. Maday, N. C. Nguyen, and A. T. Patera, Comptes Rendus Mathematique **339**, 667 (2004).

[52] J. Antoniadis *et al.*, Science **340**, 6131 (2013), arXiv:1304.6875 [astro-ph.HE].

[53] K. Lazaridis *et al.*, Mon. Not. R. Astron. Soc. **400**, 805 (2009), arXiv:0908.0285 [astro-ph.GA].

[54] G. Desvignes *et al.*, Mon. Not. Roy. Astron. Soc. **458**, 3341 (2016), arXiv:1602.08511 [astro-ph.HE].

[55] J. Antoniadis, T. M. Tauris, F. Özel, E. Barr, D. J. Champion, and P. C. C. Freire, (2016), arXiv:1605.01665 [astro-ph.HE].

[56] D. Mata Sánchez, A. G. Istrate, M. H. van Kerkwijk, R. P. Breton, and D. L. Kaplan, Mon. Not. R. Astron. Soc. **494**, 4031 (2020), arXiv:2004.02901 [astro-ph.HE].

[57] P. C. C. Freire, N. Wex, G. Esposito-Farèse, J. P. W. Verbiest, M. Bailes, B. A. Jacoby, M. Kramer, I. H. Stairs, J. Antoniadis, and G. H. Janssen, Mon. Not. Roy. Astron. Soc. **423**, 3328 (2012), arXiv:1205.1450 [astro-ph.GA].

[58] K. Liu *et al.*, Mon. Not. Roy. Astron. Soc. **499**, 2276 (2020), arXiv:2009.12544 [astro-ph.HE].

[59] I. Cognard *et al.*, Astrophys. J. **844**, 128 (2017), arXiv:1706.08060 [astro-ph.HE].

[60] T. Damour and J. H. Taylor, Astrophys. J. **366**, 501 (1991).

[61] I. S. Shklovskii, Soviet Astronomy **13**, 562 (1970).

[62] P. J. McMillan, Mon. Not. Roy. Astron. Soc. **465**, 76 (2017), arXiv:1608.00971 [astro-ph.GA].

[63] J. M. Weisberg and Y. Huang, Astrophys. J. **829**, 55 (2016), arXiv:1606.02744 [astro-ph.HE].

[64] A. D. Cameron *et al.*, Mon. Not. Roy. Astron. Soc. **475**, L57 (2018), arXiv:1711.07697 [astro-ph.HE].

[65] D. Foreman-Mackey, D. W. Hogg, D. Lang, and J. Goodman, Publ. Astron. Soc. Pac. **125**, 306 (2013), arXiv:1202.3665 [astro-ph.IM].

[66] J. H. Taylor, in *General Relativity and Gravitation* (1987) pp. 209–222.

[67] J. H. Taylor and J. M. Weisberg, Astrophys. J. **345**, 434 (1989).

[68] J. M. Lattimer, Annual Review of Nuclear and Particle Science **62**, 485 (2012), arXiv:1305.3510 [nucl-th].

[69] S. De, D. Finstad, J. M. Lattimer, D. A. Brown, E. Berger, and C. M. Biwer, Phys. Rev. Lett. **121**, 091102 (2018), [Erratum: Phys.Rev.Lett. 121, 259902 (2018)], arXiv:1804.08583 [astro-ph.HE].

[70] W. Del Pozzo and A. Vecchio, Mon. Not. Roy. Astron. Soc. **462**, L21 (2016), arXiv:1606.02852 [gr-qc].

[71] A. Gelman and D. B. Rubin, Statist. Sci. **7**, 457 (1992).

[72] R. Nan, D. Li, C. Jin, Q. Wang, L. Zhu, W. Zhu, H. Zhang, Y. Yue, and L. Qian, Int. J. Mod. Phys. D **20**, 989 (2011), arXiv:1105.3794 [astro-ph.IM].

[73] M. Kramer, D. C. Backer, J. M. Cordes, T. J. W. Lazio, B. W. Stappers, and S. Johnston, New Astron. Rev. **48**, 993 (2004), arXiv:astro-ph/0409379.

[74] L. Shao *et al.*, PoS **AASKA14**, 042 (2015), arXiv:1501.00058 [astro-ph.HE].